Theor Chem Account (2008) 119:231–244
DOI 10.1007/s00214-006-0235-9

REGULAR ARTICLE

An IEF-PCM study of solvent effects on the Faraday $\mathcal{B}$ term of MCD

Harald Solheim · Luca Frediani · Kenneth Ruud · Sonia Coriani

Received: 28 September 2006 / Accepted: 8 December 2006 / Published online: 17 February 2007

Abstract We present the first theoretical investigation of solvent effects on the Faraday $\mathcal{B}$ term of magnetic circular dichroism (MCD) at the density–functional level of theory. In our model, the solvent is described by the polarizable continuum model in its integral-equation formulation. We present the extensions required for including electron correlation effects using density–functional theory (DFT) as well as the necessary extensions for including the effects of a dielectric continuum. The new code is applied to the study of the Faraday $\mathcal{B}$ term of MCD in a series of benzoquinones. It is demonstrated that electron correlation effects, as described by DFT, are essential in order to recover the experimentally observed signs of the $\mathcal{B}$ term. Dielectric continuum effects increase, in general, the magnitude of the $\mathcal{B}$ term, leading to an overestimation of the experimental observations in most cases.

1 Introduction

Michael Faraday observed in 1846 that an externally applied magnetic field induction could induce optical activity in a non-chiral sample of molecules [1,2]. One important manifestation of this phenomenon is magnetic circular dichroism (MCD), in which one measures the differential absorption of left and right-circularly polarized light when a sample is subject to an external magnetic field induction. The molecular, quantum–mechanical theory of MCD dates back to the 1960s, and in particular to the work by Buckingham and Stephens [3] and by Stephens [4–7]. Despite its popularity both theoretically and experimentally during the 1970s and 1980s (see e.g. Refs. [8–26] and references therein), very few ab initio studies of MCD have been presented in the literature in the last decade [27–30]. However, recent advances [27–29,31,32] indicate a renewed and increasing interest in ab initio studies of MCD.

There are three distinct contributions to the MCD signal. The $\mathcal{A}$ term only arises in case of orbital degeneracy in the electronic ground state or in the final excited state. Although such orbitally degenerate states in general require multiconfigurational wave functions in order to be treated reliably, an extension applicable also to density–functional theory (DFT) was recently presented by Seth et al. [28]. The $\mathcal{C}$ term has some similarities to the $\mathcal{A}$ term and will be non-vanishing only for an orbitally degenerate electronic ground state. The last contribution, which is the only one observable for molecules without orbital degeneracies, is the $\mathcal{B}$ term, which is due to the induced magnetic moment arising because of the applied external field. To some extent, this term can be viewed as analogous to the differential absorption of right- and left-circularly polarized light measured in electronic circular dichroism spectroscopy for chiral molecules. In MCD, however, the chirality is induced by the externally applied static magnetic field, and MCD can thus be used to study the nature of excited states also for non-chiral molecules.

In this paper we extend our previous work on the Faraday $\mathcal{B}$ term of MCD [27] to the density–functional level of theory, building on recent advances made in

H. Solheim · L. Frediani · K. Ruud (✉)
Department of Chemistry, University of Tromsø,
9037 Tromsø, Norway
e-mail: kenneth.ruud@chem.uit.no

S. Coriani
Dipartimento di Scienze Chimiche, Università di Trieste,
Via L. Giorgieri 1, 34127 Trieste, Italy

the development of quadratic response theory in DFT [33,34]. DFT has proven to be an efficient way of including electron correlation effects in quantum chemical calculations. However, several recent studies have highlighted the difficulties faced by modern exchange–correlation functionals in treating excited states, and in particular states of Rydberg or charge-transfer character [35–37]. In addition to applying DFT to the study of the $\mathcal{B}$ term of MCD for the first time, we will, in this paper, also explore the quality of modern exchange–correlation functionals for the calculation of the MCD $\mathcal{B}$ term. Of particular interest to us will be the so-called Coulomb-attenuated functionals [38–40] that have proven to be quite successful in the study of higher-order non-linear optical properties [41,42].

We will, in this paper, also present the extension of the quadratic response theory for the polarizable continuum model in its integral-equation formulation (IEF-PCM) to the calculation of the Faraday $\mathcal{B}$ term of MCD. We have recently presented the extension of IEF-PCM to quadratic response theory [43] and applied it to the study of two-photon absorption cross sections [44], a process closely related to the MCD $\mathcal{B}$ term from a computational point of view. We will demonstrate that the formal differences between the MCD $\mathcal{B}$ term and a two-photon absorption cross section do not affect the implementation of the IEF-PCM, and that the inclusion of solvent effects through such a continuum model is therefore straightforward.

We will apply this new formalism to the study of the MCD $\mathcal{B}$ term in a series of benzoquinones, as there are experimental data available for these molecules in fairly innocuous solvents. Furthermore, one of these molecules, *para*-benzoquinone, was included in our previous study at the Hartree–Fock level of theory [27]. In that study, we were unable to recover the correct sign of the MCD $\mathcal{B}$ term. At the same time, we showed, using multiconfigurational self-consistent field wave functions, that electron correlation effects were important in determining the $\mathcal{B}$ term of ethene. It is therefore clearly of interest to see whether the inclusion of electron correlation effects will recover the experimental sign of the dominant transition in *para*-benzoquinone, and to what extent a dielectric continuum model improves the agreement with experiment. As DFT allows for electron correlation effects to be included at a fairly modest cost, we have also included a few larger benzoquinones for which experimental data are also available.

The rest of the paper is organized as follows. In the next section we outline the main features of our MCD implementation at the DFT level of theory, building heavily on our previous work for Hartree–Fock wave functions. We will also briefly describe the key features of the IEF-PCM in MCD $\mathcal{B}$ term calculations. In Sect. 3 we summarize the details of our calculations, and in Sect. 4 we present our results. Finally, we give some concluding remarks and an outlook.

2 Theory and implementation

2.1 Definitions

The complex optical rotation per unit path length of plane-polarized light traveling through a sample in the Z direction of a space-fixed frame is related to the complex polarizability $\tilde{\alpha}_{\alpha\beta}$ of the sample (frequency argument implied) [3,45]

$$\tilde{\phi} = \phi - i\theta = \frac{1}{4}\omega\mu_0 cN[i\langle\tilde{\alpha}_{XY} - \tilde{\alpha}_{YX}\rangle], \tag{1}$$

where $\langle\ldots\rangle$ indicates an appropriate statistical average.

In the non-absorptive region of the sample, the complex polarizability $\tilde{\alpha}_{\alpha\beta}$ is defined as

$$\begin{aligned}\tilde{\alpha}_{\alpha\beta} &= \frac{2}{\hbar}\left\{\sum_{j\neq n}\frac{\omega_{jn}}{\omega_{jn}^2-\omega^2}\Re(\langle n|\mu_\alpha|j\rangle\langle j|\mu_\beta|n\rangle)\right.\\ &\qquad\left.+\,i\sum_{j\neq n}\frac{\omega}{\omega_{jn}^2-\omega^2}\Im(\langle n|\mu_\alpha|j\rangle\langle j|\mu_\beta|n\rangle)\right\}\\ &\equiv \alpha_{\alpha\beta} - i\alpha'_{\alpha\beta} = \tilde{\alpha}^*_{\beta\alpha},\end{aligned} \tag{2}$$

where μ_α is the electric dipole moment operator, and Eq. (1) reduces to

$$\phi = -\frac{1}{2}\omega\mu_0 cN\Im\langle\tilde{\alpha}_{XY}\rangle = \frac{1}{2}\omega\mu_0 cN\langle\alpha'_{XY}\rangle\,. \tag{3}$$

These definitions are readily generalized to the absorptive regions by introducing the line-shape functions f and g—see for example Ref. [45]. For simplicity, we here restrict ourselves to the non-absorptive region.

In the presence of an external magnetic field of strength B (as occuring in MCD), the polarizability $\alpha'_{\alpha\beta}(B)$ is expanded according to

$$\alpha'_{\alpha\beta}(B) = \alpha'_{\alpha\beta}(0) + \alpha'^{(m)}_{\alpha\beta,\gamma}B_\gamma + \mathcal{O}(B^n). \tag{4}$$

Implicit summation over repeated indices is assumed here and throughout. Note that if the molecule is in a non-degenerate electronic state the zero and even order terms in the magnetic field of the above expansion vanish.

The sum-over-state expression for the higher-order polarizability $\alpha'^{(m)}_{\alpha\beta,\gamma}$ is obtained from the sum-over-state expression of $\alpha'_{\alpha\beta}$ by substituting the magnetic field-dependent eigenstates j,n and their frequency separations $\omega_{jn} = \omega_j - \omega_n$ by the corresponding perturbational

expansions in terms of zero-field eigenstates and frequency separations [45,46]

$$\begin{aligned}\alpha'^{(m)}_{\alpha\beta,\gamma} &= -\frac{2}{\hbar^2}\sum_{j\neq n}\left\{\frac{2\omega\omega_{jn}}{(\omega_{jn}^2-\omega^2)^2}(m_\gamma^j-m_\gamma^n)\Im(\langle n|\mu_\alpha|j\rangle\langle j|\mu_\beta|n\rangle)\right.\\ &+\frac{\omega}{(\omega_{jn}^2-\omega^2)}\Im\left[\sum_{k\neq n}\frac{\langle k|m_\gamma|n\rangle}{\omega_{kn}}\Big(\langle n|\mu_\alpha|j\rangle\langle j|\mu_\beta|k\rangle\right.\\ &-\langle n|\mu_\beta|j\rangle\langle j|\mu_\alpha|k\rangle\Big)+\sum_{k\neq j}\frac{\langle j|m_\gamma|k\rangle}{\omega_{kj}}\\ &\left.\left.\times\Big(\langle n|\mu_\alpha|j\rangle\langle k|\mu_\beta|n\rangle-\langle n|\mu_\beta|j\rangle\langle k|\mu_\alpha|n\rangle\Big)\right]\right\}\\ &= -\frac{2}{\hbar}\sum_{j\neq n}\left\{\frac{2\omega\omega_{jn}}{\hbar(\omega_{jn}^2-\omega^2)^2}A'^{(jn)}_{\alpha\beta\gamma}+\frac{\omega}{(\omega_{jn}^2-\omega^2)}B'^{(jn)}_{\alpha\beta\gamma}\right\}. \quad (5)\end{aligned}$$

Here m_γ is a Cartesian component of the magnetic dipole operator and $m_\gamma^k = \langle k|m_\gamma|k\rangle$. The states n,j,k and the frequency separations $\omega_{kn},\omega_{kj},\omega_{jn}$ now refer to the unperturbed system. The orientational effect on the magnetic moment is accounted for either by means of a classical weighted Boltzmann average with the potential energy $U=-m_\gamma^n B_\gamma$ or by means of an unweighted quantum statistical average [45]. For a fluid sample, the resulting rotation with respect to the molecular frame becomes [45]

$$\phi=\frac{1}{12}\omega\mu_0 cNB_z\varepsilon_{\alpha\beta\gamma}\left(\alpha'^{(m)}_{\alpha\beta,\gamma}+\frac{1}{kT}m_\gamma^n\alpha'_{\alpha\beta}\right)=V(\omega)B_z, \quad (6)$$

where we have introduced the Verdet constant $V(\omega)=\phi/B_z$. The symbol $\varepsilon_{\alpha\beta\gamma}$ denotes the Levi–Civita tensor. Note that if n is the ground state, the second term in parentheses vanishes for closed-shell systems as the permanent magnetic dipole moment is zero.

The (averaged) Faraday $\mathcal{A}$, $\mathcal{B}$ term and $\mathcal{C}$ terms, used to rationalize the MCD, can be defined from the tensors in Eq. (6) by splitting the total rotation (or more rigorously the complex rotation) into contributions from individual "transitions" $n\to j$. According to the current convention [45,47]

$$\phi=\sum_{j\neq n}\phi(n\to j) \quad (7)$$

$$\begin{aligned}\phi(n\to j) &= -\frac{\mu_0 cNB_z}{3\hbar}\left\{\frac{2\omega^2\omega_{jn}}{\hbar\left(\omega_{jn}^2-\omega^2\right)^2}\mathcal{A}\right.\\ &\left.+\frac{\omega^2}{\omega_{jn}^2-\omega^2}\left[\mathcal{B}+\frac{\mathcal{C}}{kT}\right]\right\}. \quad (8)\end{aligned}$$

Assuming that for our system of interest the transition occurs between non-degenerate n and j states, the only surviving Faraday term in Eq. (8) is the $\mathcal{B}$ term

$$\begin{aligned}\mathcal{B}(n\to j) &= \varepsilon_{\alpha\beta\gamma}\Im\left[\sum_{k\neq n}\frac{\langle k|m_\gamma|n\rangle}{\hbar\omega_{kn}}\langle n|\mu_\alpha|j\rangle\langle j|\mu_\beta|k\rangle\right.\\ &\left.+\sum_{k\neq j}\frac{\langle j|m_\gamma|k\rangle}{\hbar\omega_{kj}}\langle n|\mu_\alpha|j\rangle\langle k|\mu_\beta|n\rangle\right], \quad (9)\end{aligned}$$

which exists irrespective of the degeneracy of the ground and excited states and therefore describes the MCD of an electronic transition $n\to j$ in a molecule without degeneracies in the ground or final electronic states.

As for the first electric hyperpolarizability, $\alpha'^{(m)}_{\alpha\beta,\gamma}$ [and thus the Verdet constant $V(\omega)$] can be computed from the appropriate quadratic response function (see for instance Refs. [48,49,31]). Similarly, the $\mathcal{B}(n\to j)$ term can be rewritten and evaluated in terms of the first residue of the quadratic response function [50,27]. The identification is carried out by comparing Eq. (9) with the spectral representation expression for the first residue [50] (in atomic units)

$$\begin{aligned}&\lim_{\omega\to\omega_j}(\omega-\omega_j)\langle\!\langle\mu_\beta;m_\gamma,\mu_\alpha\rangle\!\rangle_{0,\omega}\\ &=-\sum_{k\neq n}\left[\frac{\langle n|\mu_\beta|k\rangle\langle k|\bar{m}_\gamma|j\rangle}{\omega_{kj}}+\frac{\langle n|m_\gamma|k\rangle\langle k|\bar{\mu}_\beta|j\rangle}{\omega_{kn}}\right]\langle j|\mu_\alpha|n\rangle\\ &=M^{\mu_\beta m_\gamma}_{n\leftarrow j}(0)M^{\mu_\alpha}_{j\leftarrow n}, \quad (10)\end{aligned}$$

where $M^{\mu_\alpha}_{j\leftarrow n}$ and $M^{\mu_\beta m_\gamma}_{n\leftarrow j}(0)$ indicate one- and two-photon transition matrix elements between state n and state j, respectively.

Due to the antisymmetric nature of the magnetic dipole moment operator, $m_\beta^{ll}=0,\ \forall\ l$, and $\overline{m}_\beta = m_\beta - m_\beta^{nn}\equiv m_\beta$. Assuming that the condition $k\neq j$ can be enforced in the first term of Eq. (10), the $\mathcal{B}$ term may be written as [27]

$$\mathcal{B}(n\to j)=-i\varepsilon_{\alpha\beta\gamma}\left(\lim_{\omega\to\omega_j}(\omega-\omega_j)\langle\!\langle\mu_\beta;m_\gamma,\mu_\alpha\rangle\!\rangle_{0,\omega}\right). \quad (11)$$

Computationally, the expression for the $\mathcal{B}$ term as a single residue of a quadratic response function is more convenient than the sum-over-states expression, as the explicit summations over "intermediate" excited states can be removed, and only linear equations need to be solved [50,51]. Each second-order transition moment $M^{\mu_\beta m_\gamma}_{n\leftarrow j}(0)$ in Eq. (10) is obtained by carrying out a linear transformation (summation over repeated indices

implied)

$$-\sum_{k\neq n}\left[\frac{\mu_\beta^{nk}\overline{m}_\gamma^{kj}}{\omega_k-\omega_j}+\frac{m_\gamma^{nk}\overline{\mu}_\gamma^{kj}}{\omega_k}\right]=-N_k^{\mu_\beta}(\omega_j)B_{kl}^{[2]}X_{lj}$$
$$-N_k^{m_\gamma}(0)\left[A_{kl}^{[2]}+A_{lk}^{[2]}\right]X_{lj}+N_k^{\mu_\beta}(\omega_j)\Big(E_{kml}^{[3]}+E_{klm}^{[3]}$$
$$-\omega_j S_{klm}^{[3]}\Big)N_m^{m_\gamma}(0)X_{lj}, \tag{12}$$

where the excitation vector $\boldsymbol{X}_j$ for the final state $|j\rangle$ and the response vectors $\boldsymbol{N}^Y(\omega_Y)$ for the different operators are obtained solving:

$$\left[\boldsymbol{E}^{[2]}-\omega_j\boldsymbol{S}^{[2]}\right]\boldsymbol{X}_j=0, \tag{13}$$

$$\boldsymbol{N}^{\mu_\beta}(\omega_j)=\left[\boldsymbol{E}^{[2]}-\omega_j\boldsymbol{S}^{[2]}\right]^{-1}\boldsymbol{A}^{[1]^\dagger}, \tag{14}$$

$$\boldsymbol{N}^{m_\gamma}(0)=\left[\boldsymbol{E}^{[2]}\right]^{-1}\boldsymbol{B}^{[1]}. \tag{15}$$

$\boldsymbol{E}^{[2]}$ and $\boldsymbol{S}^{[2]}$ are the generalizations of the RPA Hessian and metric matrices, respectively. $\boldsymbol{A}^{[n]}$ refers to the operator μ_β and $\boldsymbol{B}^{[n]}$ to the operator m_γ. For their definition, as well as the definition of $\boldsymbol{E}^{[n]}$ and $\boldsymbol{S}^{[n]}$, see Refs. [34, 50,51]. The first-order transition moment $M_{j\leftarrow n}^{\mu_\alpha}$ can be obtained from the residue of the linear response function [50,34] and is computed as $C_j^{[1]}=\boldsymbol{C}^{[1]}\cdot\boldsymbol{X}_j$, where C refers the operator μ_α. The first- and second-order transition moments are evaluated simultaneously and multiplied directly, which allows us to identify the sign for the $\mathcal{B}$ term unambiguously.

The implementation of the $\mathcal{B}$ term at the DFT level is then analogous to the one presented at the Hartree–Fock and MCSCF levels [27] and follows directly from the implementation of the two-photon absorption cross-sections described in Ref. [34].

Note that unphysical divergencies could occur in the linear response equation Eq. (14) when k matches the final state j [27]. Care has to be taken to solve the linear equation in a space orthogonal to the resonant excitation [27]. The singularity can be avoided a priori via a derivative reformulation, see Ref. [31].

2.2 Solvation method

Solvent effects have been included in the calculations using the Integral-Equation Formulation of the Polarizable Continuum Model [52–54]. The general principle of continuum models used for describing solvent effects is to discard the structure of the solvent and let it be described by a structureless medium bearing several properties such as a dielectric constant ϵ and a refractive index η. These properties of the medium are then used to model the solute–solvent interactions. The solute is placed in a cavity C made in the infinite continuum. The IEF-PCM allows the cavity to be modeled after the solute structure using a set of interlocking spheres which are in general centered on all or some of the solute nuclei. The formalism allows several different environments such as anisotropic or ionic media to be modeled at a uniform level of theory. For a detailed account of the model we refer to the recent review of Tomasi et al. [55] and references therein. Here we will limit ourselves to illustrate the salient features of the method and describe the key elements of the formalism needed for the calculation of medium effects on MCD.

The inclusion of solvent effects is achieved through a monoelectronic operator $\hat{Y}$ and a formally bielectronic operator $\hat{X}$ which are added to the gas-phase Hamiltonian $\hat{H}_0$, so that the Hamiltonian for an IEF-PCM solute reads

$$\hat{H}=\hat{H}_0+\hat{Y}+X(\hat{\Psi}). \tag{16}$$

The monoelectronic term $\hat{Y}$ takes into account the interaction of the electrons with the solvent reaction field generated by the nuclei, whereas the bielectronic term $\hat{X}$ describes the self-interaction of the electrons with the solvent reaction field generated by the electron density. Given a pair of molecular orbitals χ_μ and χ_ν, the solvent terms of the Hamiltonian can be written

$$Y_{\mu\nu}=\int_{\Gamma_C}V_{\mu\nu}(\boldsymbol{s})q^N(\boldsymbol{s})\,\mathrm{d}\boldsymbol{s}=\sum_\tau V_{\mu\nu,\tau}q_\tau^N$$
$$=\sum_{\tau\sigma}V_{\mu\nu,\tau}D_{\tau\sigma}(\epsilon)^{-1}V_\sigma^N, \tag{17}$$

$$X_{\mu\nu}(\Psi)=\int_{\Gamma_C}V_{\mu\nu}(\boldsymbol{s})q^e(\boldsymbol{s},\Psi)\,\mathrm{d}\boldsymbol{s}=\sum_\tau V_{\mu\nu,\tau}q_\tau^e(\Psi)$$
$$=\sum_{\tau\sigma}V_{\mu\nu,\tau}D_{\tau\sigma}(\epsilon)^{-1}V_\sigma^e(\Psi). \tag{18}$$

In these equations, Γ_C is the cavity boundary, $\boldsymbol{s}$ is a point on the boundary, $V_{\mu\nu}$ is the electrostatic potential produced by the charge density $\rho_{\mu\nu}(\boldsymbol{r})=\chi_\mu(\boldsymbol{r})\chi_\nu(\boldsymbol{r})$, q^N is the apparent surface charge (ASC) describing the polarization of the medium due to the nuclear charge, and $q^e(\Psi)$ is the ASC due to the electronic density associated with the wave function Ψ. As shown in the equations, the integral equations are solved by discretizing the cavity boundary into small portions (called tesserae), allowing for the integral to be expressed as a sum of contributions from each tessera τ. The discretization allows the ASCs q_τ^N and q_τ^e to be expressed in terms of the corresponding nuclear and electronic potentials V_σ^N and $V_\sigma^e(\Psi)$ calculated on each representative point $\boldsymbol{s}_\sigma$ of the corresponding tessera. The matrix transformation $\boldsymbol{D}(\epsilon)$

depends on the geometry of the cavity and, for a homogeneous isotropic medium, on the dielectric constant (ϵ) of the solvent.

At the SCF and MCSCF levels of theory, the wave function of the solute is obtained by minimizing the free energy of the solute

$$G = \min \frac{\left\langle \Psi \left| \hat{G} \right| \Psi \right\rangle}{\langle \Psi | \Psi \rangle}, \tag{19}$$

where $\hat{G} = \hat{H}_0 + \hat{Y} + 1/2\hat{X}$. This approach has been developed within a second-quantization formalism by Cammi et al. [56], and later extended to the treatment of linear response properties [57]. We recently presented the theory for quadratic response functions in the IEF-PCM formalism [43]. The solvent effects are introduced into the response formalism in the same way as for the energy calculation, by adding the relevant solute–solvent interaction terms into the Hamiltonian, which is then employed in the response equations (13–15). By making use of the same formalism as in the previous section, the solvent contributions can be written as follows:

$$\boldsymbol{G}^{[n]} = \boldsymbol{E}^{[n]} + \sum_{i=1}^{n} \boldsymbol{V}^{[i]} \cdot \boldsymbol{q}^{[n-i]}. \tag{20}$$

For a detailed derivation of each term we refer the reader to the original paper [43]. Suffice it to note here that for the treatment of MCD, the solvent effects do not require any further development once $\boldsymbol{G}^{[n]}$ ($n = 1, 2, 3$) is employed in the response calculations instead of its gas-phase counterpart $\boldsymbol{E}^{[n]}$, as already implemented for the calculation of single residues of the quadratic response function in order to obtain the transition moments of a Two-Photon Absorption process [44]. The modifications to the response formalism needed for the determination of the $\mathcal{B}$ term of MCD do not involve the Hamiltonian itself (to which the IEF-PCM formalism introduces new contributions), but rather the handling of the response vectors. The extension of the quadratic response theory for the IEF-PCM formalism to the case of MCD is therefore straightforward. Moreover, although the theory has originally been devised for wave function methods, it can also be employed at the Kohn–Sham DFT level: at the implementational level there is again no difference, since both HF and DFT employ the same SCF solver and the solvation terms are seamlessly introduced into DFT calculations.

We conclude this section by mentioning that, when a time-dependent field is interacting with the molecular system, the non-equilibrium formalism [58] has to be used, especially for polar solvents, in order to take into account the solvent dynamics. For a discussion of the non-equilibrium formalism we refer to Cammi and Tomasi [58], whereas the implementation at the quadratic response level can be found in Ref. [43]. Here we briefly recall that within a non-equilibrium formalism, the charges $\boldsymbol{q}^{[j]}$ in Eq. (20) are obtained from the corresponding potentials by making use of $\boldsymbol{D}(\epsilon_{\text{opt}})$ instead of $\boldsymbol{D}(\epsilon)$ for $j > 0$, where ϵ_{opt} is the square of the refractive index η of the solvent employed. Non-equilibrium effects are significant only for polar solvents where $\epsilon_{\text{opt}} \ll \epsilon$, but can be neglected for non-polar solvents where $\epsilon_{\text{opt}} \approx \epsilon$.

3 Computational details

We have calculated the Faraday $\mathcal{B}$ term of MCD for *para*-benzoquinone (pBQ), tetrachloro-*para*-benzoquinone (TCpBQ), *ortho*-benzoquinone (oBQ) and tetrachloro-*ortho*-benzoquinone (TCoBQ) at the Hartree–Fock and DFT levels of theory using the aug-cc-pVDZ and aug-cc-pVTZ basis sets. The structures of the four investigated molecules are displayed in Fig. 1. Calculations have been done both in gas phase and in *n*-hexane for pBQ, acetonitrile for TCpBQ and oBQ, and cyclohexane for TCpBQ. At the DFT level of theory, we have included several functionals: the hybrid functionals B3LYP [59,60], CAM-B3LYP [40] and BHLYP [61], and the generalized gradient approximation (GGA) functionals BLYP [62], KT1, KT2 [63] and KT3 [64]. For pBQ, TCpBQ and TCoBQ, we have also investigated the dependency of the MCD strengths (and excitation energies) on the parameters defining the CAM-B3LYP functional.

Molecular geometries have been optimized in the gas phase and in solvent at the DFT/B3LYP level of theory using the cc-pVTZ basis set. All molecules are kept planar and lie in the yz plane. For pBQ and TCpBQ the O–O axis is placed along the z axis, and for oBQ and TCoBQ the z axis is located between the oxygen atoms. The origin of the coordinate system was in all cases placed in the center of mass of the chosen molecule. Note that the *para*-benzoquinones belong to the D_{2h} point group and their $\mathcal{B}$ term is therefore gauge-origin independent irrespective of the approximations in the computational approach. For the *ortho* ones (point group symmetry C_{2v}), on the other hand, the results are gauge-origin dependent and will thus refer to the center of mass of the system.

As stated in Sect. 2.2, the solvent is in the IEF-PCM described as an infinite, polarizable continuum, and the solute molecule is placed in a cavity generated in this continuum. This cavity is on our calculations made from interlocking spheres centered on the nuclei of the heavy

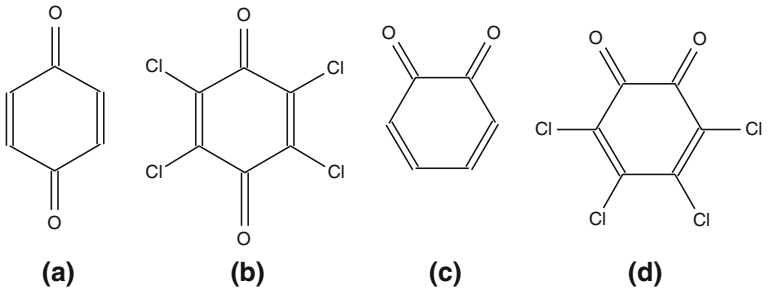

Fig. 1 Structures of molecules investigated in the present work: **a** *para*-benzoquinone (pBQ); **b** tetrachloro-*para*-benzoquinone (TCpBQ); **c** *ortho*-benzoquinone (oBQ); **d** tetrachloro-*ortho*-benzoquinone (TCoBQ)

atoms of the solute. The chosen radii are the van der Waals ones ($r_C = 1.7$ Å, $r_O = 1.52$ Å, $r_{Cl} = 1.8$ Å). For carbon atoms bonded to hydrogen, a slightly bigger sphere is used ($r_{C-H} = 1.9$ Å) in order to accommodate the hydrogen atom. All radii are multiplied by a common factor $\alpha = 1.2$.

For the non-polar solvents *n*-hexane ($\epsilon = 1.89$) and cyclohexane ($\epsilon = 2.02$), equilibrium solvation has been used. For acetonitrile, the non-equilibrium formalism has been used, with the values $\epsilon_{\text{stat}} = 36.64$ and $\epsilon_{\text{opt}} = 1.81$ for the static and the optical dielectric constants, respectively. It is worth mentioning that in the present context, where a combination of static and frequency dependent fields is employed in the experiment, a rigorous approach should make use of a "mixed" response formalism: equilibrium response for the static field and non-equilibrium response for the time-dependent fields. Such a formalism is not available at present, nor is it possible to perform a finite difference calculation with respect to the magnetic field, since the DALTON program [65] is not able to handle the corresponding imaginary perturbation as for instance done by Honda et al. [29]. We have therefore decided to employ a full non-equilibrium formalism for calculations in acetonitrile: we are confident that this approximation leads only to a small underestimation of the solvent effect whereas the use of equilibrium solvation would instead produce a significant overestimation of the effect.

Our results for the Faraday $\mathcal{B}$ term are compared to those derived from long-wavelength spectra recorded by Meier and Wagnière [22]. In order to make this comparison, the "method of moments" [5] is employed, according to which the "experimental" $\mathcal{B}$ term is derived from the recorded spectrum using the following relation:

$$\mathcal{B} = -(1/33.53) \int_{\text{band}} \frac{[\theta]_M}{\nu} \, \mathrm{d}\nu. \tag{21}$$

In the previous equation, $[\theta]_M$ is the molar ellipticity per unit magnetic field-often given in the units: degrees dl $\mathrm{dm}^{-1}\,\mathrm{G}^{-1}\,\mathrm{mol}^{-1}$—and ν is the frequency. $\mathcal{B}$ is usually reported in units of $\mathrm{D}^2\,\mu_B/\mathrm{cm}^{-1}$ or $\mathrm{D}^2\,\mu_B/\mathrm{eV}^{-1}$. Note that the validity of this approach for obtaining the $\mathcal{B}$ terms from experiment is limited if there is a strong overlap between bands corresponding to different electronic transitions.

All calculations have been performed using a local version of the DALTON program [65]. Only electronic excitations have been considered. The Faraday $\mathcal{B}$ term results are reported in atomic units (au). Note that 1 au of $\mathcal{B}$ ($a_0^4\, e^3\, \hbar^{-1}$) is $5.887644 \times 10^{-5}\ \mathrm{D}^2\,\mu_B/\mathrm{cm}^{-1}$.

4 Results and discussion

4.1 Para-benzoquinone (pBQ)

Meier and Wagnière [22] have recorded the long-wavelength MCD spectrum of pBQ in an *n*-hexane solution at 293 K. They identified two negative $\mathcal{B}$ terms in this spectral region. For the stronger band at 241 nm $\mathcal{B}$ was estimated to be −0.68 au, using the method of moments, and for the weaker band, corresponding to the dipole–forbidden transition at 280 nm, it was estimated to be −0.02 au. Ab initio calculations of the strongest band by Coriani et al. [27], using Hartree–Fock response theory and the aug-cc-pVDZ basis set, gave a $\mathcal{B}$ term value of +6.04 au. According to the authors, the neglect of solvent effects or the lack of electron correlation could be the reason why the calculation did not even give the correct sign for the MCD intensity.

MCD $\mathcal{B}$ term results for this lowest-lying dipole-allowed $X\ ^1A_g \rightarrow 1\ ^1B_{1u}(z)$ transition are collected in Table 1. The Hartree–Fock aug-cc-pVDZ result differs somewhat from the result of Coriani et al. [27] because we use a B3LYP/cc-pVTZ optimized geometry, whereas their calculation was done using an experimental geometry [66]. We note that Hartree–Fock gives a positive $\mathcal{B}$ term in both gas phase and solvent, with the value increasing from +6.78 to +8.73 au for the aug-cc-pVTZ basis when going from the gas phase to the solvent. DFT, on the other hand, gives the correct negative sign for all the functionals we have considered, and this holds both for the gas phase and the solvent calculations. Among the hybrid functionals (B3LYP, CAM-B3LYP

Table 1 *Para*-benzoquinone (pBQ). Excitation wavelength in nm and MCD $\mathcal{B}$ term in au in gas phase and, in parenthesis, *n*-hexane for the $X\,^1A_g \rightarrow 1\,^1B_{1u}$ transition. The molecule is in the *yz* plane with the *z* axis along the OO axis. B3LYP/cc-pVTZ optimized geometry in gas phase and solvent

	aug-cc-pVDZ		aug-cc-pVTZ	
	Wavelength	$\mathcal{B}$ term	Wavelength	$\mathcal{B}$ term
Hartree–Fock	203 (211)	6.23 (8.08)	203 (211)	6.78 (8.73)
B3LYP	250 (275)	−3.89 (−4.60)	251 (257)	−3.75 (−4.41)
CAM-B3LYP	233 (240)	−2.42 (−2.50)	234 (240)	−2.21 (−2.20)
BHLYP	226 (234)	−1.56 (−1.34)	227 (234)	−1.31 (−0.99)
BLYP	280 (277)	−3.96 (−6.51)	279 (278)	−3.88 (−6.12)
KT1	269 (275)	−2.91 (−4.93)	269 (275)	−2.66 (−4.68)
KT2	269 (275)	−5.36 (−5.08)	269 (275)	−4.76 (−4.88)
KT3	269 (275)	−4.85 (−5.38)	269 (275)	−4.74 (−5.27)
Experiment (Ref. [22])			(241)	(−0.68)

Table 2 *Para*-benzoquinone (pBQ). Contributions to the $\mathcal{B}$ term in au in gas phase and in *n*-hexane for the $X\,^1A_g \rightarrow 1\,^1B_{1u}$ transition with the aug-cc-pVTZ basis set. The molecule is in the *yz* plane with the *z* axis along the OO axis. B3LYP/cc-pVTZ optimized geometry in gas phase and solvent. The $\mathcal{B}$ term is obtained as the difference of the two contributions. In parenthesis enhancement factors due to solvation on each contribution and on the $\mathcal{B}$ term are reported

	$\langle\langle \mu_z; m_y, \mu_x \rangle\rangle_{0,\omega}$			$\langle\langle \mu_y; m_z, \mu_x \rangle\rangle_{0,\omega}$			$\mathcal{B}$ term		
	Gas	Sol		Gas	Sol		Gas	Sol	
Hartree–Fock	7.24	8.71	(1.20)	0.47	−0.02	(−0.04)	6.78	8.73	(1.28)
B3LYP	3.19	4.18	(1.31)	4.50	5.16	(1.15)	−3.75	−4.41	(1.17)
CAM-B3LYP	2.58	3.44	(1.33)	4.79	5.46	(1.20)	−2.21	−2.20	(1.00)
BHLYP	1.75	2.46	(1.41)	5.51	6.87	(1.24)	−1.31	−0.99	(0.75)

and BHLYP) investigated here, B3LYP gives the highest value in gas phase, −3.75 au using the aug-cc-pVTZ basis, CAM-B3LYP is slightly lower with −2.21 au and BHLYP is the lowest with −1.31 au. When including solvent effects, the B3LYP value is increased to −4.41 au, the CAM-B3LYP remains almost constant with −2.20 au and the BHLYP value decreases to −0.99 au. BHLYP in solvent gives the best agreement with the experimental estimate (cf. −0.68 au).

In a recent study of the MCD $\mathcal{B}$ term, Honda et al. [29] reported results for pBQ and oBQ. They used a GUHF/SECI wave function [29], with the Huzinaga–Dunning DZ and DZP basis sets [67]. The calculations of the $\mathcal{B}$ term were performed using both the sum-over-states (SOS) method and the finite perturbation (FP) approach. For the $^1A_g \rightarrow 1\,^1B_{1u}(z)$ transition in pBQ they report a value of −4.13 au (DZ basis set) using the SOS method (including all intermediate states), and −4.20 au (DZ) and −4.03 (DZP) using the FP method. Our response theory calculations, which includes orbital relaxation gives a positive sign for this transition using Hartree–Fock, and electron correlation is necessary to get the correct negative sign. This might indicate that the negative sign for this transition in the study by Honda et al. is the result of a fortuitous cancellation of errors since their calculation includes neither orbital relaxation nor electron correlation effects.

4.2 Tetrachloro-para-benzoquinone (TCpBQ)

The experimental MCD spectrum of TCpBQ obtained in acetonitrile [22] has a weak positive band around 370 nm, a positive band around 285 nm and a stronger negative band that stretches out of the spectral region around 170–180 nm. This last band has a shoulder around 230 nm. Meier and Wagnière identify the weak band around 370 nm as a dipole-forbidden $^1A_g \rightarrow {}^1B_{3g}$ transition. The positive band around 285 nm is identified as a $^1A_g \rightarrow {}^1B_{1u}$ transition. They do not discuss the negative band that stretches out of the spectral range. Note that a positive band corresponds to a negative $\mathcal{B}$ term, see Eq. (21).

Hartree–Fock and DFT results for the $X\,^1A_g \rightarrow 1\,^1B_{1u}$ transition are reported in Table 3. We see that Hartree–Fock gives the wrong sign for the $\mathcal{B}$ term of the first transition, predicting a positive value both in gas phase and in solvent. DFT again gives the correct sign, with the strength of the band increasing from BHLYP to CAM-B3LYP, B3LYP, KT3, KT2, KT1 and BLYP. This trend is the same both in gas phase and in solvent, but the

Table 3 Tetrachloro-*para*-benzoquinone (TCpBQ). Excitation wavelength in nm and MCD $\mathcal{B}$ term in au in gas phase and, in parenthesis, acetonitrile for the $X\ ^1A_g \rightarrow 1\ ^1B_{1u}$ transition. The molecule is in the *yz* plane with the *z* axis along the OO axis. B3LYP/cc-pVTZ optimized geometry in gas phase and solvent

	aug-cc-pVDZ		aug-cc-pVTZ	
	Wavelength	$\mathcal{B}$ term	Wavelength	$\mathcal{B}$ term
Hartree–Fock	218 (225)	1.12 (1.68)	219 (225)	1.42 (1.80)
B3LYP	325 (330)	−10.37 (−13.89)	325 (331)	−10.38 (−13.98)
CAM-B3LYP	280 (286)	−8.00 (−10.48)	280 (287)	−8.03 (−10.54)
BHLYP	266 (272)	−7.61 (−9.85)	266 (273)	−7.62 (−9.87)
BLYP	384 (390)	−13.62 (−16.34)	385 (391)	−13.02 (−16.31)
KT1	373 (379)	−11.22 (−15.05)	374 (380)	−11.17 (−15.06)
KT2	373 (379)	−11.00 (−14.75)	374 (380)	−10.95 (−14.82)
KT3	374 (379)	−10.90 (−14.62)	374 (379)	−10.82 (−14.57)
Experiment (Ref. [22])			(285)	(−4.25)

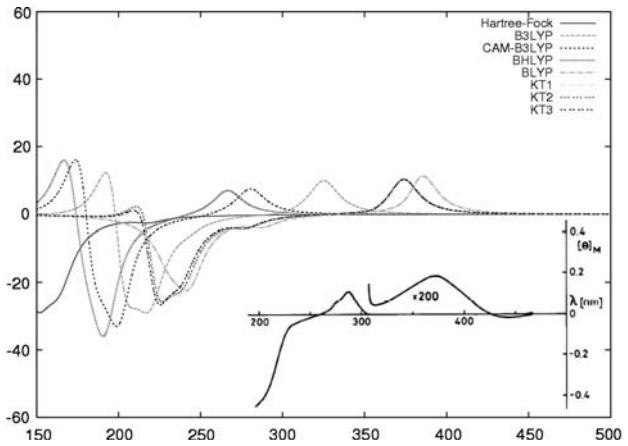

Fig. 2 Simulated MCD spectra of tetrachloro-*para*-benzoquinone (TCpBQ) in gas phase. Wavelength in nm. Lorentzian bandwidth 8 nm. Units on the ordinate axis are arbitrary. Basis set aug-cc-pVTZ. B3LYP/cc-pVTZ optimized geometry. The *inset* shows the experimental spectrum from Ref. [22]

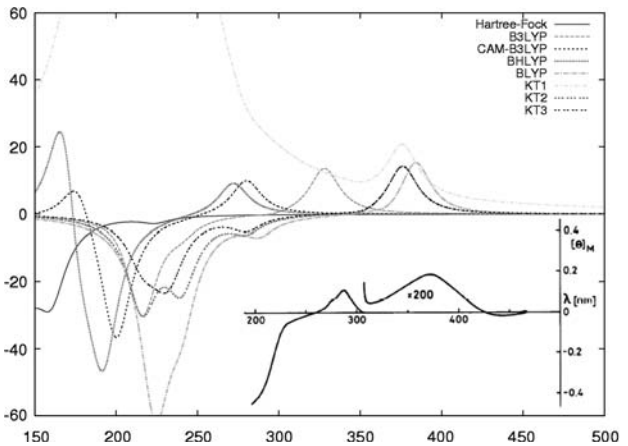

Fig. 3 Simulated MCD spectra of tetrachloro-*para*-benzoquinone (TCpBQ) in acetonitrile. Wavelength in nm. Lorentzian bandwidth 8 nm. Units on the ordinate axis are arbitrary. Basis set aug-cc-pVTZ. B3LYP/cc-pVTZ optimized geometry. The *inset* shows the experimental spectrum from Ref. [22]

strength is consistently higher in solvent. All our results for this transition are higher than the experimental estimate of −4.25 au, the closest once again being BHLYP with −7.62 au in gas phase and −9.87 au in solvent (aug-cc-pVTZ), followed by CAM-B3LYP with −8.03 au in gas phase and −10.54 au in solvent.

The strong negative band stretching outside the experimental spectral range consists of several transitions lying quite close in energy. This makes the relative weight of the transitions uncertain, and we typically see a very large positive $\mathcal{B}$ term for one transition which to a large extent is canceled by a large negative value for another transition. For this reason we do not report the $\mathcal{B}$ terms of the individual transitions, but refer to the simulation of the spectrum shown in Fig. 2 for the gas phase and in Fig. 3 for acetonitrile solution. The spectra are simulated by plotting $(-\mathcal{B})$ against the excitation wavelength in nm, and using a Lorentzian bandwidth of 8 nm. The units on the ordinate axis are arbitrary.

For the overall band structure, both Hartree–Fock and DFT predict a negative sign in agreement with experiment, with the exception of KT1 in solvent. Comparing the various DFT spectra, we see that the trends for this band in the gas phase are opposite to what is observed for the first positive band, with BHLYP predicting the strongest band and BLYP the weakest. As for the positive band, the strength increases when solvent effects are included. The trends are the same as for the gas phase, with the exception of BLYP which now has the strongest band, and KT1 which has a very strong, unphysical positive band. Considering the relative strength of the two bands—taking into account that the peak of the negative band is just outside the spectral region of the experiment—it seems that BHLYP and

Table 4 *Ortho*-benzoquinone (oBQ). Excitation wavelength in nm and MCD $\mathcal{B}$ term in au in gas phase and, in parenthesis, acetonitrile for the $X\,^1A_1 \rightarrow 1\,^1B_2$ transition. The molecule is in the *yz* plane with the *z* axis between the O atoms. B3LYP/cc-pVTZ optimized geometry in gas phase and solvent

	aug-cc-pVDZ		aug-cc-pVTZ	
	Wavelength	$\mathcal{B}$ term	Wavelength	$\mathcal{B}$ term
B3LYP	400 (441)	−3.66 (−5.04)	400 (442)	−3.68 (−5.08)
CAM-B3LYP	366 (403)	−3.71 (−5.21)	366 (403)	−3.73 (−5.25)
BHLYP	358 (393)	−3.65 (−5.20)	358 (394)	−3.67 (−5.23)
BLYP	439 (484)	−3.44 (−4.69)	439 (484)	−3.46 (−4.73)
KT1	436 (478)	−3.32 (−4.58)	437 (479)	−3.35 (−4.62)
KT2	437 (480)	−3.36 (−4.58)	438 (481)	−3.39 (−4.63)
KT3	434 (476)	−3.66 (−4.60)	435 (477)	−3.68 (−4.59)
Experiment (Ref. [22])			(380)	(−3.23)

CAM-B3LYP give the best agreement with experiment for this ratio.

4.3 Ortho-benzoquinone (oBQ)

In the experimental MCD spectrum of oBQ obtained in acetonitrile [22], Meier and Wagnière identified one positive band at about 380 nm. They assigned this band to the $X\,^1A_1 \rightarrow 1\,^1B_2$ transition, and estimated a value of −3.23 au for the $\mathcal{B}$ term.

The calculated MCD $\mathcal{B}$ term values for this transition are reported in Table 4. In the gas phase, the DFT results vary between −3.3 and −3.7 au, quite close to the experimental estimate. When including solvent effects, the magnitude of the $\mathcal{B}$ term increases for all the functionals.

For Hartree–Fock, the B3LYP optimized geometry seems to be strongly affected by instabilities in the wave function, and the results both for the excitation energies and the Faraday $\mathcal{B}$ term using this geometry are clearly not physical. Due to this, Hartree–Fock results are not included in Table 4.

We have included simulated spectra based on our calculations in Fig. 4 for the gas phase and Fig. 5 for acetonitrile solution. The main feature of the experimental spectrum [22], apart from the band discussed above, is a strong negative band stretching out of the spectral range. This feature is also shown in the simulated spectra for all the DFT functionals investigated both in the gas phase and in solvent. The fine structure between 200 and 300 nm is, however, not very well reproduced in the simulation for any of the functionals.

In the study by Honda et al. [29], the $X\,^1A_1 \rightarrow 1\,^1B_2$ transition in oBQ has an MCD $\mathcal{B}$ term value of −4.13 au (DZ) using the SOS method, and −4.20 au (DZ) and −4.03 au (DZP) using the FP method. Again their results are in qualitative agreement with experiment.

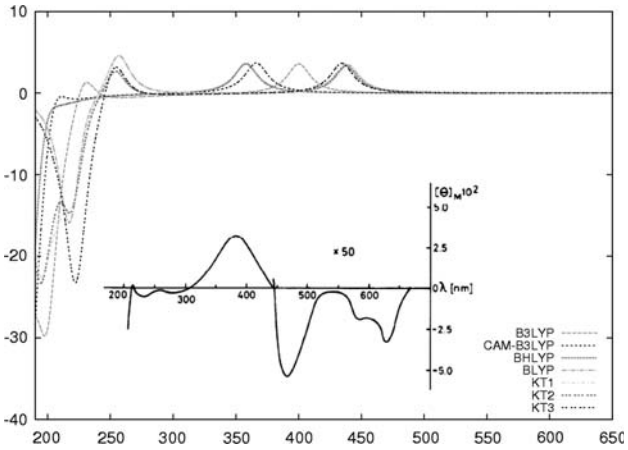

Fig. 4 Simulated MCD spectra of *ortho*-benzoquinone (oBQ) in gas phase. Wavelength in nm. Lorentzian bandwidth 8 nm. Units on the ordinate axis are arbitrary. Basis set aug-cc-pVTZ. B3LYP/cc-pVTZ optimized geometry. The *inset* shows the experimental spectrum from Ref. [22]

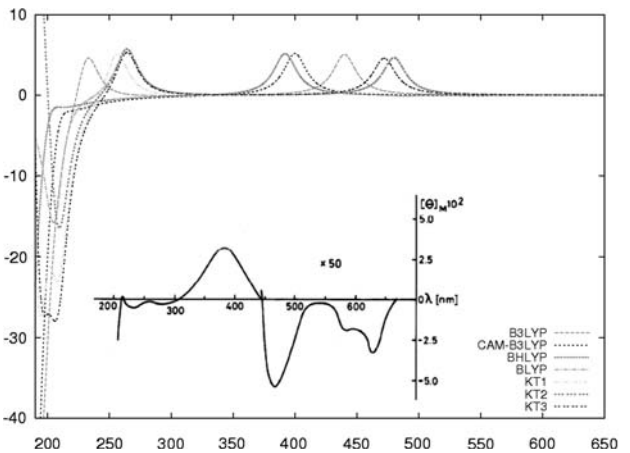

Fig. 5 Simulated MCD spectra of *ortho*-benzoquinone (oBQ) in acetonitrile. Wavelength in nm. Lorentzian bandwidth 8 nm. Units on the ordinate axis are arbitrary. Basis set aug-cc-pVTZ. B3LYP/cc-pVTZ optimized geometry. The *inset* shows the experimental spectrum from Ref. [22]

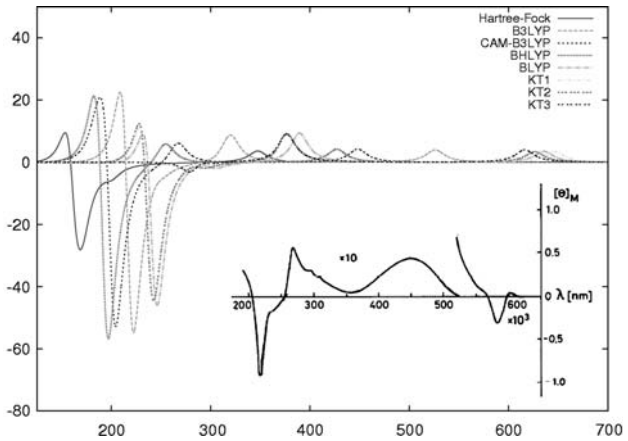

Fig. 6 Simulated MCD spectra of tetrachloro-*ortho*-benzoquinone (TCoBQ) in gas phase. Wavelength in nm. Lorentzian bandwidth 8 nm. Units on the ordinate axis are arbitrary. Basis set aug-cc-pVTZ. B3LYP/cc-pVTZ optimized geometry. The *inset* shows the experimental spectrum from Ref. [22]

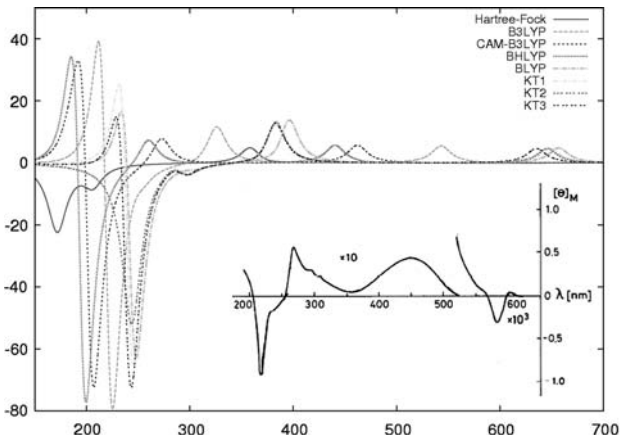

Fig. 7 Simulated MCD spectra of tetrachloro-*ortho*-benzoquinone (TCoBQ) in cyclohexane. Wavelength in nm. Lorentzian bandwidth 8 nm. Units on the ordinate axis are arbitrary. Basis set aug-cc-pVTZ. B3LYP/cc-pVTZ optimized geometry. The *inset* shows the experimental spectrum from Ref. [22]

4.4 Tetrachloro-ortho-benzoquinone (TCoBQ)

The experimental MCD spectrum of tetrachloro-*ortho*-benzoquinone obtained in cyclohexane [22] consists of a positive band at 450 nm, another positive band at about 270 nm with a shoulder at about 300 nm, and in the region 190–230 nm there is a strong bisignate signal. The bisignate signal has a negative peak at about 220 nm and a positive peak just outside the spectral range, probably at about 190 nm. There are also two very small peaks at 543 and 587 nm, which can be attributed to vibronic transitions. Meier and Wagnière attribute the longest wavelength band at 450 nm to a $^1A_1 \rightarrow ^1B_2$ transition and the band at 270 nm to a $^1A_1 \rightarrow ^1B_1$ transition.

Simulated spectra of our results are given in Fig. 6 (gas phase) and Fig. 7 (cyclohexane solution), and show that DFT again gives the same qualitative picture as the experimental data, with two positive bands and a stronger bisignate signal. This holds both for the gas phase and the solvent calculations, with the exception of KT3 in the gas phase. As for the other molecules, Hartree–Fock is not even qualitatively correct.

The calculated MCD $\mathcal{B}$ term values for the $X\,^1A_1 \rightarrow 1^1B_2$ transition are reported in Table 5. In the gas phase, all the results lie between −3.35 and −4.25 au, even at the Hartree–Fock level. B3LYP (−4.00), CAM-B3LYP (−4.24) and BHLYP (−4.24) are closest to the experimental estimate of −4.08 au. The inclusion of solvent effects increases the $\mathcal{B}$ term value, and the results are then in the range −4.65 to −5.80 au.

In Table 6 we have reported the results for the $X\,^1A_1 \rightarrow 1\,^1B_1$ transition. For this transition, Hartree–Fock gives a positive sign for the $\mathcal{B}$ term, whereas DFT gives a negative sign in agreement with experiment. When comparing with the experimental value of −3.57 au reported by Meier and Wagnière [22], we see that our gas phase values are at least twice as large. In cyclohexane we get even higher values. It should be noted that there is a strong overlap between this band and the bisignate signal in the experimental spectrum, which means that in this case the value obtained by the method of moments should be considered as a lower bound for the $\mathcal{B}$ term.

4.5 Different parameterizations of the CAM-B3LYP functional

Of the DFT functionals we have investigated so far, BHLYP and CAM-B3LYP clearly give $\mathcal{B}$ term results for the molecules in our study in best agreement with experiment. From Tables 1–6, we see that this also holds for the excitation energies. However, the strengths of the MCD bands are in general too high compared to experiment, especially for the PCM calculations. In this section we will consider how changing the parameters of the CAM-B3LYP functional affects the values of the MCD $\mathcal{B}$ term for the molecules we have considered.

The key element of a Coulomb-attenuating method such as CAM-B3LYP is the separation of the exchange into two contributions by a partitioning of the r_{12}^{-1} operator

$$\frac{1}{r_{12}} = \frac{[\alpha + \beta \mathrm{erf}(\mu r_{12})]}{r_{12}} + \frac{1 - [\alpha + \beta \mathrm{erf}(\mu r_{12})]}{r_{12}}, \qquad (22)$$

where α and β are dimensionless parameters satisfying $0 \leq \alpha \leq 1$, $0 \leq \beta \leq 1$ and $0 \leq \alpha + \beta \leq 1$, and the dimension of the parameter μ is chosen such that

Table 5 Tetrachloro-*ortho*-benzoquinone (TCoBQ). Excitation wavelength in nm and MCD $\mathcal{B}$ term in au in gas phase and, in parenthesis, cyclohexane for the $X\ ^1A_1 \rightarrow 1\ ^1B_2$ transition. The molecule is in the *yz* plane with the *z* axis between the O atoms. B3LYP/cc-pVTZ optimized geometry in gas phase and solvent

	aug-cc-pVDZ		aug-cc-pVTZ	
	Wavelength	$\mathcal{B}$ term	Wavelength	$\mathcal{B}$ term
Hartree–Fock	346 (357)	−3.70 (−5.12)	347 (357)	−3.70 (−5.18)
B3LYP	525 (542)	−3.97 (−5.41)	526 (543)	−4.00 (−5.46)
CAM-B3LYP	447 (461)	−4.20 (−5.66)	448 (462)	−4.24 (−5.72)
BHLYP	426 (439)	−4.21 (−5.70)	427 (441)	−4.24 (−5.76)
BLYP	634 (655)	−3.49 (−4.79)	636 (657)	−3.51 (−4.83)
KT1	628 (647)	−3.37 (−4.66)	629 (649)	−3.40 (−4.70)
KT2	625 (644)	−3.36 (−4.64)	626 (646)	−3.39 (−4.69)
KT3	615 (633)	−3.97 (−4.65)	616 (635)	−4.00 (−4.65)
Experiment (Ref. [22])			(450)	(−4.08)

Table 6 Tetrachloro-*ortho*-benzoquinone (TCoBQ). Excitation wavelength in nm and MCD $\mathcal{B}$ term in au in gas phase and, in parenthesis, cyclohexane for the $X\ ^1A_1 \rightarrow 1\ ^1B_1$ transition. The molecule is in the *yz* plane with the *z* axis between the O atoms. B3LYP/cc-pVTZ optimized geometry in gas phase and solvent

	aug-cc-pVDZ		aug-cc-pVTZ	
	Wavelength	$\mathcal{B}$ term	Wavelength	$\mathcal{B}$ term
Hartree–Fock	200 (205)	2.74 (5.94)	200 (206)	3.17 (6.57)
B3LYP	319 (326)	−9.09 (−12.22)	320 (326)	−9.14 (−12.32)
CAM-B3LYP	266 (272)	−7.26 (−9.09)	267 (272)	−7.31 (−9.13)
BHLYP	254 (259)	−7.29 (−8.93)	254 (260)	−7.33 (−8.95)
BLYP	388 (395)	−13.68 (−15.31)	388 (395)	−13.62 (−15.38)
KT1	376 (383)	−10.49 (−14.17)	376 (383)	−10.60 (−14.95)
KT2	376 (383)	−10.09 (−13.74)	376 (383)	−10.16 (−13.87)
KT3	376 (383)	−9.09 (−13.27)	376 (383)	−9.14 (−13.38)
Experiment (Ref. [22])			(270)	(−3.57)[a]

[a] Lower bound of the strength because of some overlap with positive band

Table 7 *Para*-benzoquinone (pBQ). Excitation wavelength in nm and MCD $\mathcal{B}$ term in au for different parameterizations of CAM-B3LYP in gas phase and, in parenthesis, *n*-hexane for the $X\ ^1A_g \rightarrow 1\ ^1B_{1u}$ transition. The molecule is in the *yz* plane with the *z* axis along the OO axis. B3LYP/cc-pVTZ optimized geometry in gas phase and solvent

	aug-cc-pVDZ		aug-cc-pVTZ	
	Wavelength	$\mathcal{B}$ term	Wavelength	$\mathcal{B}$ term
$\alpha = 0.19\ \beta = 0.46\ \mu = 0.33$	233 (240)	−2.42 (−2.50)	234 (240)	−2.21 (−2.20)
$\alpha = 0.2\ \beta = 0.3\ \mu = 0.4$	235 (242)	−2.73 (−2.93)	235 (242)	−2.54 (−2.65)
$\alpha = 0.2\ \beta = 0.45\ \mu = 0.4$	228 (237)	−1.97 (−1.88)	228 (235)	−1.74 (−1.56)
$\alpha = 0.2\ \beta = 0.8\ \mu = 0.4$	214 (222)	0.24 (0.97)	215 (222)	0.58 (1.42)
$\alpha = 0.2\ \beta = 0.8\ \mu = 0.3$	224 (231)	−1.25 (−0.93)	224 (231)	−0.97 (−0.55)
$\alpha = 0.2\ \beta = 0.8\ \mu = 0.2$	237 (244)	−2.74 (−2.94)	237 (244)	−2.54 (−2.66)
Experiment (Ref. [22])			(241)	(−0.68)

(μr_{12}) is dimensionless. The first term is evaluated using a modified expression for exact orbital exchange, and the second term is evaluated using the Becke88 exchange functional [62].

The parameters of the CAM-B3LYP functional [40] were obtained by setting $\mu = 0.33$ as recommended by Tawada et al. [68], and optimizing α and β through a fitting to atomization energies for a set of molecules. The optimized values, keeping μ fixed, are $\alpha = 0.19$ and $\beta = 0.46$. Recent studies by Peach et al. [69] and Peach and Tozer [70] have shown that this parameterization is not optimal for all properties. In particular, this parameterization does not satisfy the exact long-range exchange condition

$$\alpha + \beta = 1, \tag{23}$$

Table 8 Tetrachloro-*para*-benzoquinone (TCpBQ). Excitation wavelength in nm and MCD $\mathcal{B}$ term in au for different parameterizations of CAM-B3LYP in gas phase and, in parenthesis, acetonitrile for the X $^1A_g \rightarrow 1\ ^1B_{1u}$ transition. The molecule is in the *yz* plane with the *z* axis along the OO axis. B3LYP/cc-pVTZ optimized geometry in gas phase and solvent

	aug-cc-pVDZ		aug-cc-pVTZ	
	Wavelength	$\mathcal{B}$ term	Wavelength	$\mathcal{B}$ term
$\alpha = 0.19\ \beta = 0.46\ \mu = 0.33$	280 (286)	−8.00 (−10.48)	280 (287)	−8.03 (−10.54)
$\alpha = 0.2\ \beta = 0.3\ \mu = 0.4$	286 (292)	−8.60 (−11.30)	286 (292)	−7.79 (−11.37)
$\alpha = 0.2\ \beta = 0.45\ \mu = 0.4$	271 (277)	−7.48 (−9.70)	272 (278)	−6.94 (−9.74)
$\alpha = 0.2\ \beta = 0.8\ \mu = 0.4$	245 (251)	−4.22 (−5.32)	245(252)	−4.16 (−5.21)
$\alpha = 0.2\ \beta = 0.8\ \mu = 0.3$	261 (267)	−5.96 (−7.69)	261(268)	−5.42 (−7.67)
$\alpha = 0.2\ \beta = 0.8\ \mu = 0.2$	285 (292)	−8.08 (−10.65)	286 (292)	−7.35 (−10.72)
Experiment (Ref. [22])			(285)	(−4.25)

Table 9 Tetrachloro-*ortho*-benzoquinone (TCoBQ). Excitation wavelength in nm and MCD $\mathcal{B}$ term in au for different parameterizations of CAM-B3LYP in gas phase and, in parenthesis, cyclohexane for the X $^1A_1 \rightarrow 1\ ^1B_2$ transition. The molecule is in the *yz* plane with the *z* axis between the O atoms. B3LYP/cc-pVTZ optimized geometry in gas phase and solvent

	aug-cc-pVDZ		aug-cc-pVTZ	
	Wavelength	$\mathcal{B}$ term	Wavelength	$\mathcal{B}$ term
$\alpha = 0.19\ \beta = 0.46\ \mu = 0.33$	447 (461)	−4.20 (−5.66)	448 (462)	−4.24 (−5.72)
$\alpha = 0.2\ \beta = 0.3\ \mu = 0.4$	457 (471)	−4.17 (−5.63)	458 (473)	−4.21 (−5.69)
$\alpha = 0.2\ \beta = 0.45\ \mu = 0.4$	432 (445)	−4.18 (−5.62)	433 (446)	−4.22 (−5.68)
$\alpha = 0.2\ \beta = 0.8\ \mu = 0.4$	385 (397)	−4.02 (−5.36)	387 (398)	−4.06 (−5.42)
$\alpha = 0.2\ \beta = 0.8\ \mu = 0.3$	414 (426)	−4.18 (−5.60)	415 (428)	−4.23 (−5.76)
$\alpha = 0.2\ \beta = 0.8\ \mu = 0.2$	459 (473)	−4.24 (−5.73)	460 (475)	−4.29 (−5.80)
Experiment (Ref. [22])			(450)	(−4.08)

Table 10 Tetrachloro-*ortho*-benzoquinone (TCoBQ). Excitation wavelength in nm and MCD $\mathcal{B}$ term in au for different parameterizations of CAM-B3LYP in gas phase and, in parenthesis, cyclohexane for the X $^1A_1 \rightarrow 1\ ^1B_1$ transition. The molecule is in the *yz* plane with the *z* axis between the O atoms. B3LYP/cc-pVTZ optimized geometry in gas phase and solvent

	aug-cc-pVDZ		aug-cc-pVTZ	
	Wavelength	$\mathcal{B}$ term	Wavelength	$\mathcal{B}$ term
$\alpha = 0.19\ \beta = 0.46\ \mu = 0.33$	266 (272)	−7.26 (−9.09)	267 (272)	−7.31 (−9.13)
$\alpha = 0.2\ \beta = 0.3\ \mu = 0.4$	274 (280)	−7.74 (−9.89)	275 (280)	−7.79 (−9.96)
$\alpha = 0.2\ \beta = 0.45\ \mu = 0.4$	257 (263)	−6.91 (−8.43)	258 (263)	−6.94 (−8.44)
$\alpha = 0.2\ \beta = 0.8\ \mu = 0.4$	227 (233)	−3.69 (−3.17)	228 (233)	−3.57 (−2.93)
$\alpha = 0.2\ \beta = 0.8\ \mu = 0.3$	244 (249)	−5.45 (−6.02)	244 (250)	−5.42 (−5.91)
$\alpha = 0.2\ \beta = 0.8\ \mu = 0.2$	270 (276)	−7.31 (−9.17)	271 (276)	−7.35 (−9.21)
Experiment (Ref. [22])			(270)	(−3.57)[a]

[a] Lower bound of the strength because of some overlap with positive band

which is especially important for charge-transfer and Rydberg excitations [69].

For this reason, we have also considered some other parameterizations of the CAM-B3LYP functional. In addition to the regular CAM-B3LYP parameterization, we have considered three parameterizations suggested in the study by Peach and Tozer [70], one of which satisfies the long-range exchange condition. These functionals are supplemented with two more functionals that also satisfy this condition, but where we have modified the value of μ. The parameterizations are listed with the corresponding excitation energies and MCD $\mathcal{B}$ term values in Table 7 for pBQ, Table 8 for TCpBQ and Tables 9 and 10 for TCoBQ. For oBQ we experienced for some of the parameterizations, using a B3LYP optimized geometry, the same kind of instabilities that we observed for the Hartree–Fock wave function (see Sec. 4.3). We have therefore chosen not to report any results for this molecule.

The MCD $\mathcal{B}$ term results for the X $^1A_1 \rightarrow 1\ ^1B_2$ transition in TCoBQ (Table 9), do not vary much. For the other transitions reported, there is a wide varia-

tion among the functionals, but the parameterization, $\alpha = 0.2$, $\beta = 0.8$, $\mu = 0.3$, gives the best overall results compared to experiment. Both the gas phase and PCM results are in good agreement with the experimental estimates, and especially for PCM there is a marked improvement compared to the functionals we have considered in the previous sections.

This parameterization gives, however, in general too high excitation energies, and for this quantity, the regular CAM-B3LYP functional ($\alpha = 0.19$, $\beta = 0.46$, $\mu = 0.33$) is consistently in better agreement with the experimental data. It still appears difficult to find a functional that can reproduce both the excitation energies and the MCD $\mathcal{B}$ terms with high accuracy.

4.6 Solvent effect and correlation

We have noted that the solvent sometimes leads to a reduction of the final $\mathcal{B}$ term. For instance, for pBQ with the BHLYP functional and the aug-cc-pVTZ basis set a reduction (in absolute value) from -1.31 in gas-phase to -0.99 in solvent is observed. The same trend is observed with BHLYP/aug-cc-pVDZ and for a particular choice of the CAM-B3LYP parametrization ($\alpha = 0.2$, $\beta = 0.8$, $\mu = 0.3$) with both basis sets. For TCoBQ this happens with CAM-B3LYP ($\alpha = 0.2$, $\beta = 0.8$, $\mu = 0.4$).

Although this contrasts with the common sense of an amplification of a property due to solvation, it should be kept in mind that according to Eq. (11), $\mathcal{B}$ is the sum of several contributions with alternating signs. In particular, for pBQ there are two contributions coming from the response functions $\langle\langle \mu_z; m_y, \mu_x \rangle\rangle_{0,\omega}$ and $\langle\langle \mu_y; m_z, \mu_x \rangle\rangle_{0,\omega}$, respectively. We have reported these contributions in Table 2 for HF and a selection of functionals (B3LYP, CAM-B3LYP, BHLYP). As can be seen, the first contribution decreases from HF to B3LYP whereas the second increases: this behavior can easily be attributed to electron correlation effects. The solvent effect increases the magnitude of all contributions (with the exception of the second contribution for HF) and the relative enhancement (reported in parenthesis for each contribution) is bigger for a more correlated method. Moreover, the solvent effect is always bigger for the first contribution than the second. For this reason, the balance is shifted from an enhancement of the $\mathcal{B}$ term (HF, B3LYP) to an apparent absence of solvent effect (CAM-B3LYP) to a reduction of the $\mathcal{B}$ term (BHLYP). We also remark that with a simpler model, such as for instance taking solvation effects into account through the Lorentz factor $f = (\epsilon_{opt.} + 2)/3$, this behavior would not be observed.

5 Conclusions

We have presented the first theoretical investigation of solvent effects on the Faraday $\mathcal{B}$ term of magnetic circular dichroism at the density–functional level of theory. Several functionals have been investigated in our study, and inclusion of correlation effects have been shown to be crucial in order to get even qualitative agreement with experiment.

Solvent effects are shown to be significant. Dielectric continuum effects increase in general the magnitude of the $\mathcal{B}$ term, in most cases leading to an overestimation of its value compared to the experimentally derived ones. In some cases a reduction of the $\mathcal{B}$ term upon solvation has been observed which is connected to the interplay of correlation and dielectric medium effects on the individual contributions to the final result for the different functionals employed.

At the density–functional level of theory, the $\mathcal{B}$ terms have for the molecules included in our study been shown to be very sensitive to the amount of exact orbital exchange included in the functional. CAM-B3LYP represents a marked improvement compared to B3LYP, and modifying the parameters governing the Coulomb attenuation can further improve the results.

In the present study vibronic effects have been neglected. For a full comparison with experiment, such effects should be included in addition to the solvent effects, since the experimental spectra show clear vibronic structure.

Acknowledgments It is a pleasure for us to dedicate this paper to one of the pioneers of the theoretical foundations of MCD, Professor Philip J. Stephens, on the occasion of his 65th birthday.

This work has received support from the Norwegian Research Council through a Strategic University Program in Quantum Chemistry (Grant No 154011/420), and a YFF grant to KR (Grant No 162746/V00), as well as through a grant of computer time from the Norwegian Supercomputing Program. SC acknowledges support from the Italian Ministero dell'Università e Ricerca (MUR), Progetti di Ricerca di Interesse Nazionale (PRIN2004).

References

1. Faraday M(1846) Philos Mag 28:294
2. Faraday M (1846) Philos Trans R Soc Lond. 136:1
3. Buckingham AD, Stephens PJ (1966) Ann Rev Phys Chem 17:399
4. Stephens PJ (1970) J Chem Phys 52:3489
5. Stephens PJ (1968) Chem Phys Lett 2:241
6. Stephens PJ (1974) Ann Rev Phys Chem 25:201
7. Stephens PJ (1976) Adv Chem Phys 35:197
8. Seamans L, Linderberg J (1972) Mol Phys 24:1393
9. Seamans L, Moscowitz A (1972) J Chem Phys 56:1099
10. Schatz PN, McCaffery AJ (1969) Q Rev 23:552
11. Shieh DJ, Lin SH, Eyring H (1972) J Phys Chem 76:1844

12. Shieh DJ, Lin SH, Eyring H (1973) J Phys Chem 77:1031
13. Brith M, Rowe MD, Schnepp O, Stephens PJ (1975) Chem Phys 9:57
14. Gedanken A, Schnepp O (1976) Chem Phys 12:341
15. Fuke K, Schnepp O (1979) Chem Phys 38:211
16. Fuke K, Gedanken A, Schnepp O (1979) Chem Phys Lett 67:483
17. Michl J (1978) J Am Chem Soc 100:6801
18. Michl J (1978) J Am Chem Soc 100:6812
19. Michl J (1984) Tetrahedron 40:3845
20. Obbink JH, Hezemans AMF (1976) Theor Chim Acta 43:75–87
21. Nordén B, Håkansson R, Pedersen PB, Thulstrup EW (1978) Chem Phys 33:355–366
22. Meier AR, Wagnière GH (1987) Chem Phys 113:287
23. Goldstein E, Vijaya S, Segal GA (1980) J Am Chem Soc 102:6198
24. Diamond J, Segal GA (1984) J Am Chem Soc 106:952
25. Duch V, Segal GA (1986) J Chem Phys 79:2951 [Erratum: ibid. 84:544 (1986)]
26. Piepho SB, Schatz PN (1983) Group theory in spectroscopy: with applications to magnetic circular dichroism. Wiley, New York
27. Coriani S, Jørgensen P, Rizzo A, Ruud K, Olsen J (1999) Chem Phys Lett 300:61
28. Seth M, Ziegler T, Banerjee A, Autschbach J, van Gisbergen SJA, Baerends EJ (2004) J Phys Chem 120:10942
29. Honda Y, Hada M, Ehara M, Nakatsuji H, Michl J (2005) J Chem Phys 123:164113
30. Christiansen O, Coriani S, Gauss J, Hättig C, Jørgensen P, Pawłowski F, Rizzo A (2006) Accurate NLO properties for small molecules. Methods and results. In: Papadopoulos M, Leszczynski J, Sadlej A, (eds), Nonlinear optical properties of matter: from molecules to condensed phases. Kluwer, Dordrecht
31. Coriani S, Hättig C, Jørgensen P, Helgaker T (2000) J Chem Phys 113:3561
32. Kjærgaard T, Jansik B, Jørgensen P, Coriani S, Michl J (2006) J Phys Chem (in press)
33. Sałek P, Vahtras O, Helgaker T, Ågren H (2002) J Chem Phys 117:9630
34. Sałek P, Vahtras O, Guo J, Luo Y, Helgaker T, Ågren H (2003) Chem Phys Lett 374:446
35. Bauernschmitt R, Ahlrichs R (1996) Chem Phys Lett 256:454
36. Furche F, Ahlrichs R (2004) J Am Chem Soc 124:3804
37. Pecul M, Ruud K, Helgaker T (2004) Chem Phys Lett 388:110
38. Leininger T, Stoll H, Werner H-J, Savin A (1997) Chem Phys Lett
39. Iitkura H, Tsuneda T, Yanai T, Hirao K (2001) J Chem Phys 115:3540
40. Yanai T, Tew D, Handy NC (2004) Chem Phys Lett 393:51
41. Rudberg R, Sałek P, Helgaker T, Ågren H (2001) J Chem Phys 123:184108
42. Ferrighi L, Frediani L, Cappelli C, Sałek P, Ågren H, Helgaker T, Ruud K (2006) Chem Phys Lett 425:267
43. Frediani L, Ågren H, Ferrighi L, Ruud K (2005) J Chem Phys 123:144117
44. Frediani L, Rinkevicius Z, Ågren H (2005) J Chem Phys 122:244104
45. Barron LD (2004) Molecular light scattering and optical activity, 2nd edn. Cambridge University Press, Cambridge
46. Barron LD, Buckingham AD (1972) Mol Phys 23:145
47. Michl J, Thulstrup EW (1986) Spectroscopy with polarized light. VCH Publishers, Inc., New York
48. Parkinson WA, Sauer SPA, Oddershede J, Bishop DM (1993) J Chem Phys 98:487
49. Jaszuński M, Jørgensen P, Rizzo A, Ruud K, Helgaker T (1994) Chem Phys Lett 222:263
50. Olsen J, Jørgensen P (1985) J Chem Phys 82:3235
51. Hettema H, Jensen HJA, Jørgensen P, Olsen J (1992) J Chem Phys 97:1174
52. Mennucci B, Cancés E, Tomasi J (1997) J Phys Chem B, 101:10506
53. Cancés E, Mennucci B (1998) J Math Chem 23:309
54. Cancés E, Mennucci B, Tomasi J (1997) J Chem Phys 107:3032
55. Tomasi J, Mennucci B, Cammi R (2005) Chem Rev 105:2999
56. Cammi R, Frediani L, Mennucci B, Tomasi J, Ruud K, Mikkelsen KV (2002) J Chem Phys 117:13
57. Cammi R, Frediani L, Mennucci B, Ruud K (2003) J Chem Phys 119:5818
58. Cammi R, Tomasi J (1995) Int J Quant Chem 29:465
59. Becke AD (1993) J Chem Phys 98:5648
60. Stephens PJ, Devlin FJ, Chabalowski CF, Frisch MJ (1994) J Phys Chem 98:11623
61. Becke AD (1993) J Chem Phys 98:1372
62. Becke AD (1988) Phys Rev A 38:3098
63. Keal TW, Tozer DT (2003) J Chem Phys 119:3015
64. Keal TW, Tozer DT (2004) J Chem Phys 121:5654
65. Dalton (2005) an ab initio electronic structure program, Release 2.0. See http://www.kjemi.uio.no/software/dalton/dalton.html
66. Hagen K, Hedberg K (1973) J Chem Phys 59:158
67. Huzinaga S (1971) Approximate atomic functions. Technical report, University of Alberta, Edmonton
68. Tawada Y, Tsuneda T, Yanagisawa S, Yanai T, Hirao K (2004) J Chem Phys 120:8425
69. Peach MJG, Helgaker T, Sałek P, Keal T, Lutnæs OB, Tozer DJ, Handy NC (2006) Phys Chem Chem Phys 8:558
70. Peach MJG, Cohen AJ, Tozer DJ (2006) Phys Chem Chem Phys 8:4543